

2

Submitted for the  
Seventh ASTM-EURATOM Symposium on Reactor Dosimetry  
Strasbourg, France  
August 27-31, 1990

EGG-M--89426

DE91 006101

Neutron Spectrum Studies in the ATR<sup>†</sup>

JW Rogers, R. A. Anderl and M. H. Putnam  
Idaho National Engineering Laboratory  
EG&G Idaho, Inc.  
P. O. Box 1625  
Idaho Falls, Idaho USA 84115-7111

Introduction

The Advanced Test Reactor (ATR) at the Idaho National Engineering Laboratory (INEL) has been and currently is used to provide irradiation fields to study the effects of intense radiation on samples of reactor materials. These samples include fuel, cladding, control and structural materials. The ATR is also used to irradiate target materials for the production of radionuclides used in industrial and medical applications as well as for scientific research. Routine monitoring of the "thermal" and "fast" neutron levels have been conducted during every operational cycle since its startup in 1970. The routine neutron dosimetry has been primarily accomplished using the  $^{59}\text{Co}(n,\gamma)^{60}\text{Co}$  reaction for "thermal" neutrons and the  $^{58}\text{Ni}(n,p)^{58}\text{Co}$  reaction for "fast" neutrons as described in ASTM standard methods E261, E262 and E264.<sup>1</sup> Neutron spectrum studies have now been conducted in the epithermal and fast neutron energy ranges for the various capsule irradiation test facilities and the routine neutron monitoring locations.

Description of the ATR

The ATR is a uniquely designed core with a serpentine fuel assembly arrangement (four lobes) to allow loop experiments and optimal safety and control device location (see Figure 1). The ATR is fueled with enriched uranium which is in an aluminum matrix and cladding. The forty plate type fuel assemblies have an active length of 1.22 meters and are cooled by light water which typically reaches about 75°C at normal power. The core is surrounded by a beryllium reflector and hafnium control cylinders which are used primarily to shift the core lobe power. Hafnium fixed (neck) shims are also used primarily to compensate for fuel burnup and are located inside the fuel arrangement (in H-holes or in A holes).

The loop irradiation facilities located in and between the lobes normally contain the tubing and cooling annuli necessary to allow the loops to operate at the desired loop experimental conditions. Normally six of the loops have tubular hafnium safety rod assemblies which are 98 percent

<sup>†</sup>Work performed under U. S. Department of Energy Contract No. DE-AC07-76ID01570.

MASTER

withdrawn above the core during operation. The annuli around the loops allow for some neutron spectral tailoring by the amount and type of moderators, scatterers and absorbers that are placed in them. The safety rod followers have holes (SR) in them where the routine neutron monitors are positioned during routine operation. These holes are located azimuthally around the loops at 90 degree intervals. There are numerous holes in the core and reflector regions which allow capsules to be irradiated at high neutron levels. There are capsule irradiation tanks located outside the core-reflector tank on the north (ON) and south (OS) sides which have lower neutron levels.

#### Nominal ATR Peak Fluence Rate per Lobe MW

<u>Position</u>	<u>Thermal (2200 m/s)</u>	<u>Fast (&gt;1 MeV)</u>
H-holes	7.5E12	6.0E12
A-holes	7.5E12	7.5E12
B-holes	1.5E13	4.5E12
SE(SR)-holes	9.0E12	6.0E12
I-holes	6.5E11	3.0E10
OS-5	3.0E10	2.0E9

#### Spectrum Studies Irradiation Conditions

Since the ATR normal operational cycles are too high in power and too long in duration to allow optimum exposure and measurement of the neutron monitors desirable for spectral analyses, a 10 MW - 8 hour irradiation was performed. The lobe powers were divided as follows: LNW = 1.81 MW, LNE = 1.82 MW, LC = 2.17 MW, LSW = 2.15 MW, LSE = 2.05 MW based on the N-16 lobe power monitors. The neutron monitors were centered at the reactor midplane elevation in the following locations (see Figure 1): [H2, H-10, H-14], [A-1, A-10, A-12], [\*SE(SR)-1, \*SE(SR)-3], [B-4, B-8, B-11], [I-6, I-8, I-22], OS-5

#### Sensor Materials in the Neutron Monitor Packages

The neutron monitor packages consisted of cadmium tubes with 7.2-cm outside length, 0.24-cm outside diameter, 0.14-cm inside diameter, 6.0-cm inside length and 0.6-cm crimped ends. This tube formed the encapsulation of all the neutron monitors. A capsule of this length was deemed acceptable since there is no observable axial neutron gradient for this length about the core midplane due to the overall core height of ~122 cm.

The selection, design, irradiation and handling of the sensor materials and encapsulations were based on the standard guidelines<sup>1</sup> as described

\*SE-1 is 67.7° clockwise from north and SE-3 is 247.7° clockwise from north. The hafnium control cylinders were withdrawn to about 60.5° of rotation, the hafnium fixed shims were fully inserted and the hafnium regulating rods were fully withdrawn.

in ASTM E844-86. The sensor materials were  $^{235}\text{U}$ , Sc, Au, Co,  $^{237}\text{Np}$ ,  $^{238}\text{U}$ , Ni, Fe, Ti, Cu and Al with the fission monitors encapsulated in vanadium.

### Reaction Rate Measurements

The neutron-induced, gamma-ray radioactivities of each sensor were measured by gamma-ray spectrometry using standardized and calibrated germanium detector based spectrometry systems. These spectrometer systems detection efficiencies were calibrated with an estimated uncertainty of  $\pm 2$  percent ( $1\sigma$ ) throughout the energy range of these measurements. The energy scale was calibrated to an uncertainty of  $\pm 0.1$  KeV with a photopeak resolution (FWHM) of 1.9 KeV at 1.33 MeV. In general, the methods for detector calibration and analysis of radionuclides described in ASTM Standard E181-82 were followed.<sup>1</sup>

In general, these measured reaction rates have been determined using the standard methods<sup>1</sup> as described in ASTM E261-77 and ASTM E1005-84. Where they exist, ASTM standard methods were followed for specific types of monitors and reactions. The fission reaction rates were determined from the  $^{95}\text{Zr}$ ,  $^{103}\text{Ru}$ ,  $^{140}\text{Ba}$  and  $^{140}\text{La}$  fission products observed in each fission monitor.

The total estimated uncertainties for the measured reaction rates are a combination of the detection efficiency, counting statistics, gamma-ray emission probability, fission yield and target atom uncertainty components. Uncertainties ranged from 2 percent to about 6 percent.

### Neutron Spectra Calculations

The calculated neutron spectra for the H-hole region were obtained using one-dimensional  $S_6$  transport theory and the SCAMP computer code.<sup>2</sup> To obtain these spectra, various parameters in the SCAMP model were adjusted to reproduce results from the PDQ-7 two-dimensional diffusion theory code<sup>3</sup> where the 73-group structure of SCAMP was collapsed to match the 4-group structure of PDQ-7.

These variations and adjustments were necessary in the H-hole regions because of the hafnium fixed shims which were located in some of the H-holes.

The calculated neutron spectra used for input to the analyses were obtained from the above spectrum by adjusting the magnitude with scaling factors based on the  $^{235}\text{U}$  fission rates in measurement locations.

### Multigroup Spectral Analyses

Multigroup characterization of the neutron spectra in the ATR was obtained by least-squares adjustment analyses using the FERRET<sup>4,5</sup> code as per ASTM Standard E944-83.<sup>1</sup> In these analyses, adjustment of a priori (or

input) estimates of the group fluence rates were made to achieve consistency between the average of the measured reaction rates and the reaction rates calculated using the equation:

$${}_jR_i = \sum_g {}_jC_g {}_i\sigma_g {}_j\phi_g$$

where

${}_jR_i$  = the reaction rate for reaction  $i$ , spectrum  $j$ ,

${}_jC_g$  = group correction factor to account for neutron flux depression and shielding effects due to the use of cadmium covered dosimeters, spectrum  $j$ ,

${}_i\sigma_g$  = infinite dilute group cross section for reaction  $i$ ,

${}_j\phi_g$  = group values for the neutron flux spectrum identified as spectrum  $j$ .

The analyses were made in a group structure employing 51 groups with group energy boundaries chosen to cover in some detail the major structure in the dosimeter cross sections and in the neutron spectra. Input estimates of the 51-group fluxes,  ${}_j\phi_g$ , for each core location were derived, using a spline interpolation scheme, from the 73-group calculated fluxes. The group correction factors,  ${}_jC_g$ , were obtained from the 51-group fluxes by dividing the "cadmium covered" group values by the corresponding "no cadmium" group values. Infinite-dilute group cross sections,  ${}_i\sigma_g$ , were obtained by processing 620-group representations of the dosimeter cross sections, as specified in the ENDF/B-V Dosimetry file,<sup>6</sup> into 51-group cross sections using reactor-spectrum weighting. Least-squares-adjustment analyses of the type performed here also required a detailed prescription of the covariances for the input fluxes and cross sections.

Covariances matrices were prescribed for the 51-group input cross sections and flux data. For all of the dosimeter reactions, except for  ${}^{45}\text{Sc}(n,\gamma)$  and for  ${}^{59}\text{Co}(n,\gamma)$ , the PUFF code<sup>7</sup> was used to process ENDF/B-V covariance files and to generate the appropriate 51-group covariance matrices. Because the ENDF/B-V covariance files for  ${}^{45}\text{Sc}(n,\gamma)$  and  ${}^{59}\text{Co}(n,\gamma)$  were incomplete, a covariance prescription provided by Schmittroth<sup>8</sup> was used.

A parametric expression<sup>4,5</sup> was used to generate the fractional covariance matrix elements,  $M_{ij}$ , for the input flux data using

$$M_{ij} = r_n^2 + r_i r_j \rho_{ij}$$

where  $r_n$  is a fractional normalization uncertainty (independent of groups  $i$  and  $j$ ),  $r_i$  and  $r_j$  represent fractional statistical uncertainties for groups  $i$  and  $j$ , respectively, and  $\rho_{ij}$  is the correlation matrix that correlates the group statistical uncertainties. The correlation matrix elements,  $\rho_{ij}$ , are defined by

$$\rho_{ij} = (1 - \delta) \delta_{ij} + \theta e^{-\frac{(i-j)^2}{2\gamma^2}}$$

where the first term represents a purely random component to the correlation ( $\delta_{ij} = 0$  for  $i \neq j$ , and  $\delta_{ij} = 1$  for  $i = j$ ) and the second term represents a short-range correlated component with strength  $\theta$  and range  $\gamma$ . For the present FERRET analyses, the normalization uncertainty,  $r_n$ , was estimated to be 10% and the groupwise statistical uncertainty,  $r_i$ , was estimated to be 20%, with  $\theta = 0.8$  indicating a relatively high degree of correlation in the groupwise statistical uncertainty components. Analyses were made for  $\gamma = 2$  and  $\gamma = 4$  to investigate the influence of the correlation range on the spectrum adjustment outcome where a value of 4 was found optimal. It should be noted that these uncertainty prescriptions are not rigorously derived from neutronics calculations used to obtain the a priori or input spectra. However, they are large enough to ensure that the final group flux adjustments and normalizations are largely determined by the relatively accurate dosimeter reaction rates and cross sections.

Knowledge of the various cross-section group responses are important to identifying those energy regions of the neutron spectra that are most sensitive to the specific dosimeter reactions, i.e., to identifying those regions of the neutron spectra that will be adjusted and better defined as a result of the FERRET analysis. A comparison of the fractional group responses is shown in Figure 2 for the low-energy, resonance dosimeters and in Figure 3 for the high-energy threshold dosimeters. It is important to note from Figure 3 that the threshold dosimeters provide good overlapping responses over the energy range from ~0.5 MeV to greater than 10 MeV. This means that the least-squares-adjustment analysis should provide an improved characterization of this region of the input neutron spectrum, a region of particular significance to accurate prediction of displacement damage production due to fast neutrons. The response information shown in Figure 2 illustrates significant narrow response due to resonances in the  $^{197}\text{Au}(n,\gamma)$ ,  $^{59}\text{Co}(n,\gamma)$  and  $^{58}\text{Fe}(n,\gamma)$  reaction and a generally broad response for  $^{45}\text{Sc}(n,\gamma)$  and  $^{235}\text{U}(n,f)$  reaction. These reactions should provide improved characterization of the input neutron spectrum from 0.4 eV to approximately  $10^{-3}$  MeV. The region between  $10^{-3}$  MeV and 0.5 MeV will not, in general, undergo significant improvement because no dosimeters have response in this region.

### Thermal Neutron Spectral Characteristics

The thermal neutron spectral characterizations of the ATR consist of the concept of an equivalent 2200 m/s fluence rate ( $\text{n/cm}^2/\text{sec}$ ) which is proportional to the saturated  $^{59}\text{Co}(n,\gamma)^{60}\text{Co}$  reaction rate of thermal neutrons. The thermal neutrons are those below about 0.5 eV as determined by cadmium covered and bare irradiations of effectively infinite dilute monitor material. The unperturbed thermal neutron reaction rate fractions

measured for the  $^{59}\text{Co}(n,\gamma)^{60}\text{Co}$  reaction in the ATR locations are listed below.

H-holes - $0.75 \pm 0.01$	Inner B-holes - $0.84 \pm 0.02$	OS-holes - $0.98 \pm 0.01$
A-holes - $0.75 \pm 0.01$	Outer B-holes - $0.91 \pm 0.03$	I-holes - $0.98 \pm 0.01$
SR-holes - $0.76 \pm 0.01$		

Unperturbed, in this case, means that there are only the normal reactor materials present in the holes. The dependence of these values on the positions of the hafnium control cylinders in the outer B-holes, I-holes and OS/ON holes have not been established.

#### Results of Multigroup Spectral Analyses

Complete detailed results cannot be presented here due to limited text space and will be compiled in a future publication. A typical set of data is illustrated in Figure 4 where the adjusted and unadjusted (input) group fluence rates are shown for position H-2. From this comparison it can be seen that the input group fluence rates were probably 20 to 30% too low in the low-energy region and 10 to 20% too low in the high-energy region. After adjustment the calculated-to-measured reaction rate ratios typically range from 0.98 to 1.02 for all reactions except those with the highest energy response where the ratios are typically from 0.94 to 1.06 which can be attributed to the very low reaction rates there.

A comparison of the adjusted multigroup spectra from the various locations under study is given in Figure 5. These spectra show, as expected, how the high-energy and low-energy regions change relative to each other. Since a high degree of consistency was obtained between the measured and calculated reaction rates it can be expected that these adjusted spectra represent the true spectra with less uncertainty than the unadjusted spectra.

ATR reactor-relevant spectrum-averaged cross sections were computed using the adjusted spectra from the FERRET analyses. These results are presented in Table 1. Of particular interest to ATR routine fast neutron monitoring is the 0.121 barn value for the  $^{58}\text{Ni}(n,p)$ , >1 MeV spectrum-averaged cross section in the H-hole region. The estimated uncertainty of  $\pm 4$  percent represents a factor of five reduction in the estimated uncertainty in the value routinely used (0.133 barns). In addition to providing more accurate >1 MeV spectrum-averaged cross sections, this work provides >0.1 MeV cross sections with estimated uncertainties of  $\pm 7$  percent which are relevant to neutron damage.

Displacement damage (dpa) cross-sections for Fe, Ni and Cr were also derived in this work and are presented in Table 1.

## References

1. 1988 Annual Book of ASTM Standards, Volume 12.02, "Nuclear (11), Solar, and Geothermal Energy," American Society for Testing and Materials, Philadelphia, PA (1988).
2. G. E. Putnam, TOPIC - A Fortran Program Calculating Transport of Particles in Cylinders, IDO-16968, April 1964. SCAMP is an undocumented internal  $S_n$  transport code with one-dimensional slab, cylindrical, and spherical capabilities. In cylindrical form, it is a multigroup version of TOPIC.
3. C. J. Pfeifer, PDQ-7 Reference Manual II, WAPD-TM-947(2), 1971.
4. F. Schmittroth, "FERRET Data Analysis Code," US DoE Report HEDL-TME 79-40, Hanford Engineering Development Laboratory (September 1979).
5. F. Schmittroth, Nucl. Sci. Eng., 72, (1979) 19-34.
6. R. Kinsey, "ENDF-102 Data Formats and Procedures for the Evaluated Nuclear Data File, ENDF," BNL-NCS-50496, (ENDF-102) 2nd Edition (ENDF/B-V), UC-80, (General Reactor Technology - TID-4500), Brookhaven National Laboratory, Upton, NY (October 1979).
7. "PUFF2 Determination of Multigroup Covariance Matrices from ENDF/B-V Uncertainty Files," RSIC Computer Code Collection, PSR-157 (1980).

Table 1. Spectrum-average cross sections derived from ATR H-hole FERRET analysis

Dosimeter Reaction	Spectrum-averaged Cross Sections (barns)					
	>0.4 eV		>0.1 MeV		>1.0 MeV	
	Value	$\sigma(\%)$	Value	$\sigma(\%)$	Value	$\sigma(\%)$
$^{45}\text{Sc}(n,\gamma)$	4.57E-01	5	---	---	---	---
$^{197}\text{Au}(n,\gamma)$	5.54E+01	5	---	---	---	---
$^{235}\text{U}(n,f)$	1.15E+01	5	---	---	---	---
$^{59}\text{Co}(n,\gamma)$	2.78E+00	5	---	---	---	---
$^{58}\text{Fe}(n,\gamma)$	5.25E-02	5	---	---	---	---
$^{237}\text{Np}(n,f)$	---	---	1.10E+00	7	2.27E+00	4
$^{238}\text{U}(n,f)$	---	---	1.96E-01	7	4.04E-01	4
$^{47}\text{Ti}(n,p)$	---	---	1.04E-02	7	2.14E-02	4
$^{58}\text{Ni}(n,p)$	---	---	5.87E-02	7	1.21E-01	4
$^{54}\text{Fe}(n,p)$	---	---	4.32E-02	7	8.92E-02	4
$^{46}\text{Ti}(n,p)$	---	---	5.79E-03	7	1.19E-02	4
$^{63}\text{Cu}(n,\alpha)$	---	---	2.74E-04	7	5.65E-04	4
$^{48}\text{Ti}(n,p)$	---	---	1.44E-04	7	2.89E-04	4
$^{27}\text{Al}(n,\alpha)$	---	---	3.22E-04	7	6.66E-04	4
Fe (dpa)	---	---	6.81E+02	7	1.39E+03	5
Ni (dpa)	---	---	7.18E+02	8	1.45E+03	5
Cr (dpa)	---	---	7.61E+02	7	1.55E+03	5



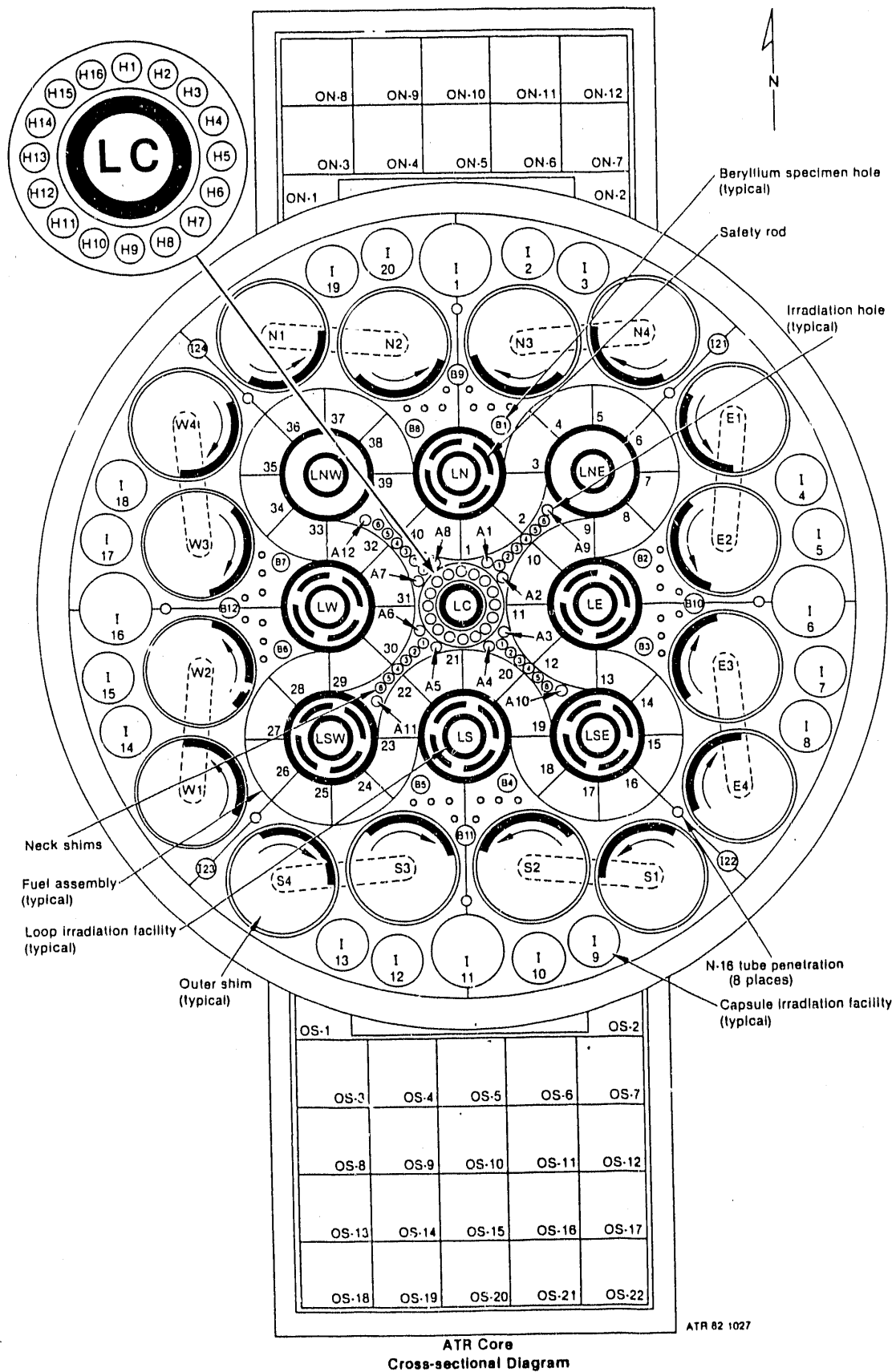


Figure 1. ATR core cross-section diagram.

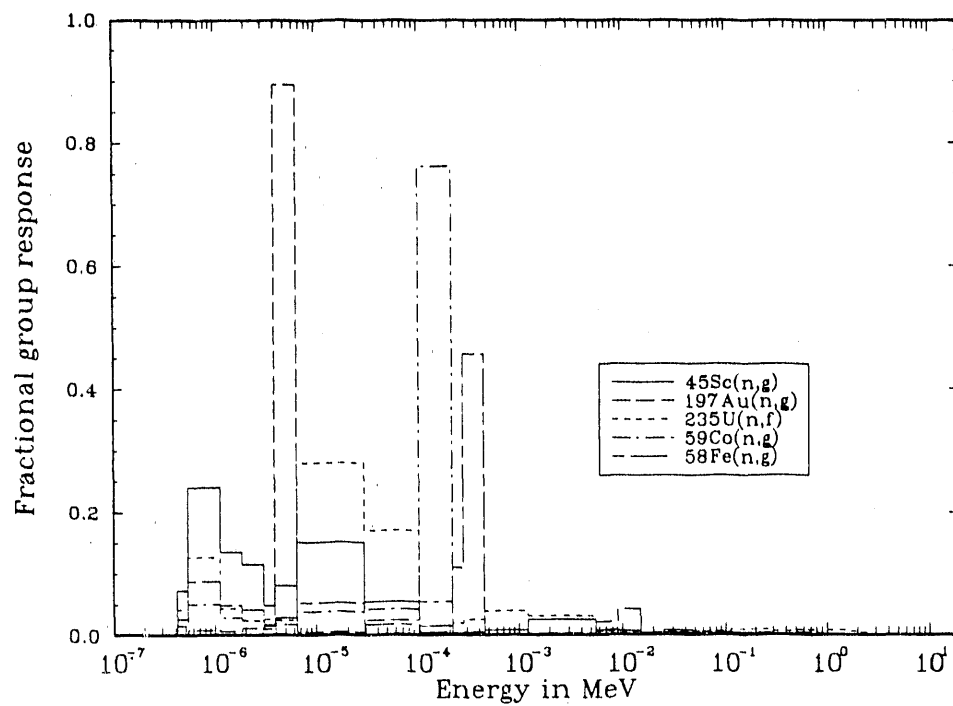


Figure 2. Typical multigroup response for low-energy dosimeter reactions.

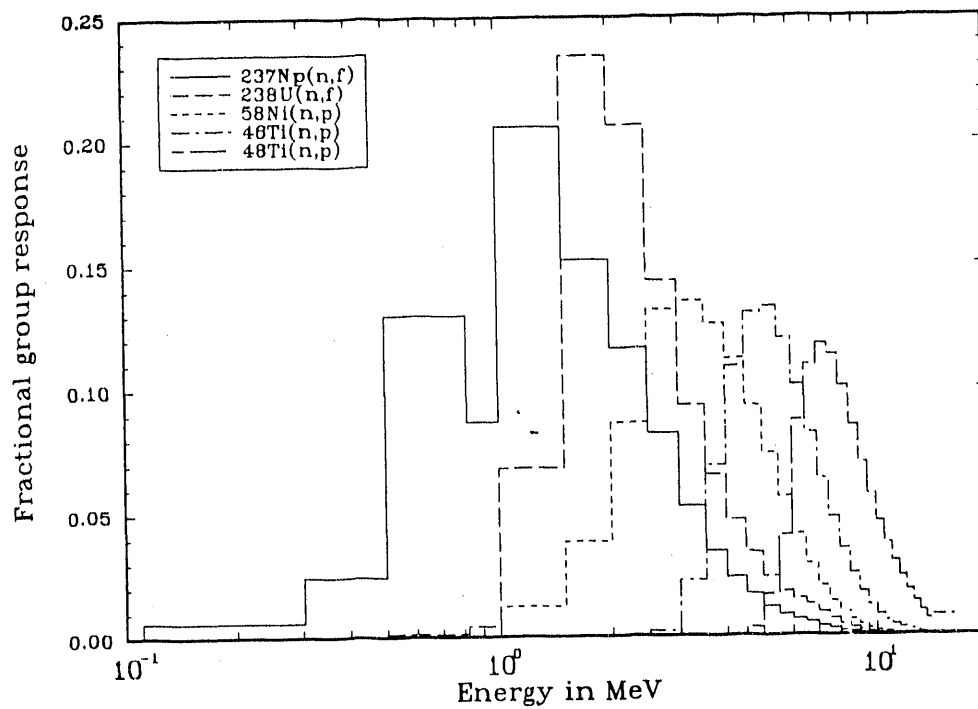


Figure 3. Typical multigroup response for high-energy threshold dosimeter reactions.

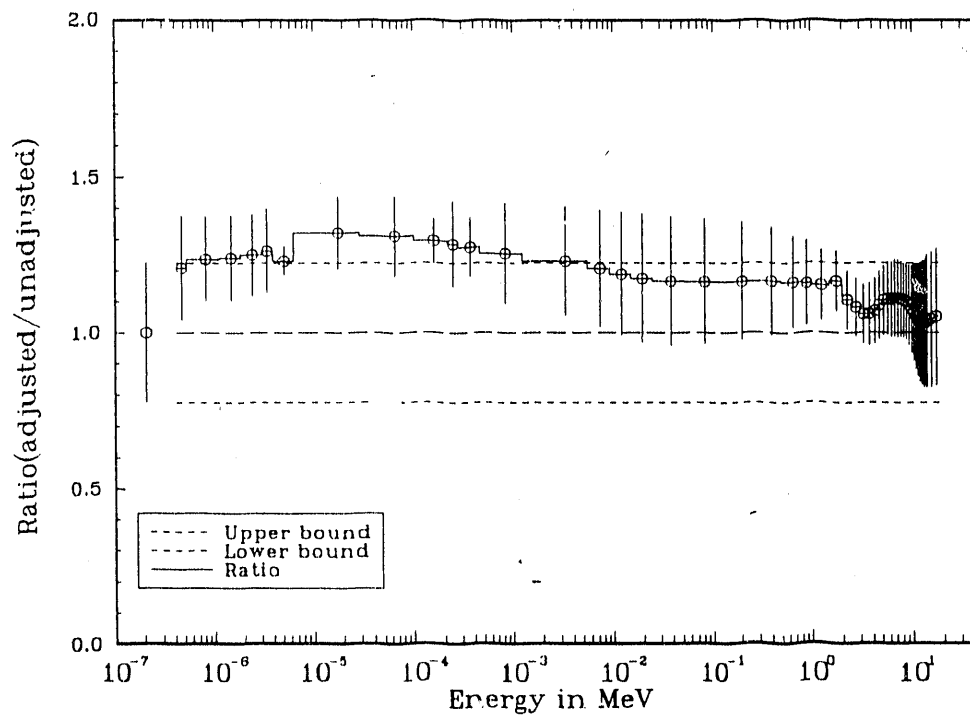
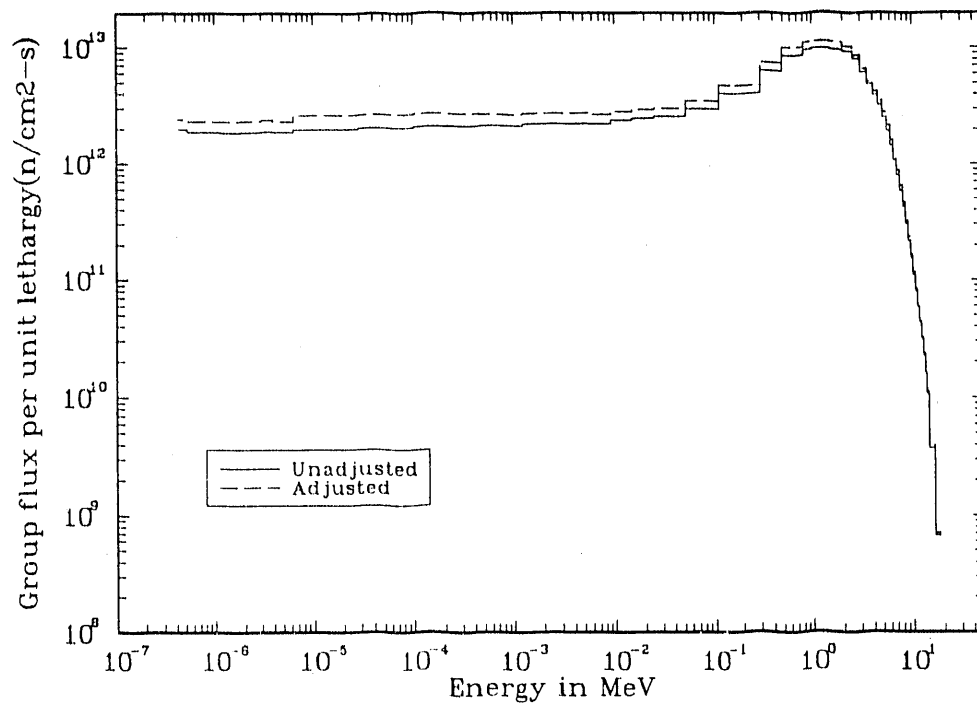


Figure 4. Comparison of adjusted and unadjusted (input) group fluence rates for H-02 location. Upper part of figure shows multigroup fluence rates. Lower part shows ratio of adjusted-to-unadjusted group values with input uncertainty bounds and final uncertainty error bars.

## DISCLAIMER

This report was prepared as an account of work sponsored by an agency of the United States Government. Neither the United States Government nor any agency thereof, nor any of their employees, makes any warranty, express or implied, or assumes any legal liability or responsibility for the accuracy, completeness, or usefulness of any information, apparatus, product, or process disclosed, or represents that its use would not infringe privately owned rights. Reference herein to any specific commercial product, process, or service by trade name, trademark, manufacturer, or otherwise does not necessarily constitute or imply its endorsement, recommendation, or favoring by the United States Government or any agency thereof. The views and opinions of authors expressed herein do not necessarily state or reflect those of the United States Government or any agency thereof.

### COMPARISON OF ATR ADJUSTED SPECTRA

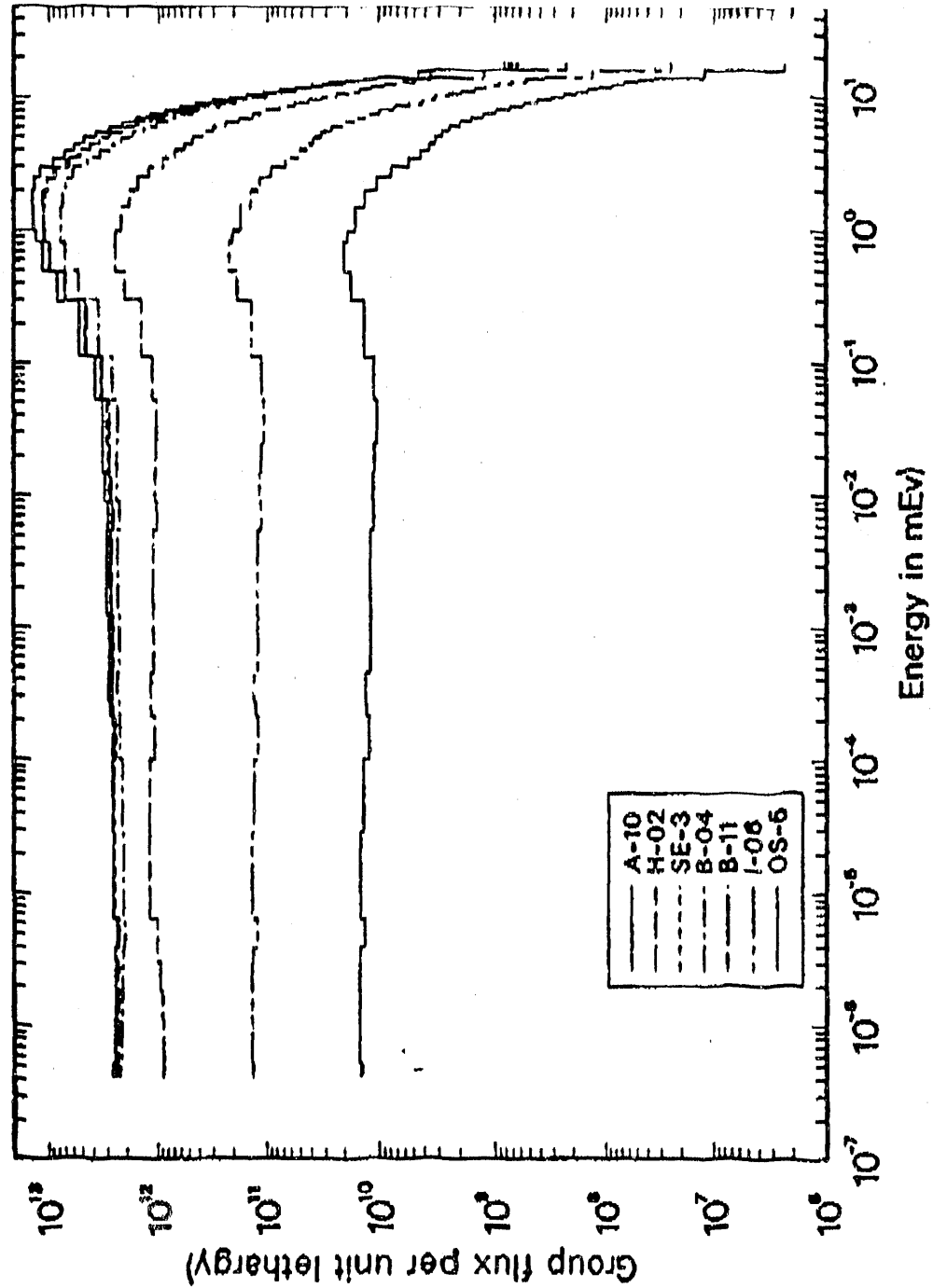


Figure 5. Comparison of final adjusted spectra for ATR locations associated with this study.

**END**

**DATE FILMED**

01 / 25 / 91

